A Relaxation Solution for Transonic Flow over Jet Flapped Airfoils

N.D. Malmuth* and W.D. Murphy†
Science Center, Rockwell International, Thousand Oaks, Calif.

Transonic small disturbance theory has been used as a framework for the development of a relaxation solution for the flow over supercritical jet flapped airfoils. The flexibility in grid refinement provided by the results obtained in this work for the far-field and asymptotic jet development affords an accurate, rapidly convergent algorithm for this problem. The use of a three grid approach and spatially variable relaxation provides a decisive enhancement in computational efficiency of the method. The structure of the far-field solution corresponds to a "vorticity packet" as the dominant term in the development. Results of the calculations for NACA 0012 and modified 64A406 airfoils indicate that the jet expands the region of supercritical flow and substantially enhances the lift. Comparisons with data of Yoshihara for a rearward cambered airfoil validates these conclusions.

Introduction

RECENT emphasis on the extension of buffet boundaries of transonic aircraft has made powered lift systems such as the jet flap an attractive possibility. The prediction of the aerodynamic performance of such devices has been investigated extensively at incompressible speeds ever since the early work of Hagedorn and Ruden.[1] Subsequent to these studies, Spence[2] developed a thin airfoil theory, which gave quantitative information on the benefits of two-dimensional jet flaps. Other workers extended the theoretical models to include three dimensionality, as well as thickness and ground effects.[3-5]

The advent of modern computational methods has made the analysis of such flows at transonic speeds an encouraging prospect. Yoshihara and his coworkers[6] have applied unsteady methods to analyze two-dimensional supercritical jet flapped airfoils. Ives and Melnik[7] treated these shapes, applying Jameson's steady-state difference methods, using mapping procedures to solve the boundary value problem for the exact potential equation on a finite domain in a half plane. The principal drawbacks of the unsteady method involve the lengthiness of the computations and difficulties in satisfying the boundary conditions. For the previous steady-state method, the limitations in mesh density inherent in the mappings have been partially responsible for difficulties involving the speed of convergence of the solution, and treatment of the trailing edge singularity.

Toward achieving a rapid and simplified procedure capable of generalization to three-dimensional flows, the authors have solved this problem within the framework of transonic small disturbance theory without recourse to mappings in creating a tractable numerical formulation. The method to be described in this paper employs the usual transfer of boundary conditions to the wind axis, using the asymptotic expansions for the velocity components to provide a self-consistent formulation and a simplification of the numerical algorithm. The analysis, which is an extension of Krupp, Murman and Cole,[8-10] treats the boundary value problem in the finite plane, using recently developed shock-point operators developed by Murman. An important feature of the present difference procedure is the fact that it provides good approximations to the Rankine Hugoniot jump conditions for nearly normal shocks through its fully conservative nature, and also allows the wave drag to be calculated accurately using methods recently presented by Murman and Cole.[11]

Computational results will be discussed showing the enhancements of the lift on NACA 0012, and 64A406 profiles, as well as a rear cambered airfoil tested by Yoshihara. As a validation, a subcritical scaled version of Spence's solution for a flat plate at $M_\infty = 0.4$ will be compared with the small disturbance solution of this paper. Supercritically, the chordwise pressures obtained from the algorithm of this paper will be compared with that developed in Ref. 7 for a NACA 0012 wing at zero incidence.

Formulation

In order to clarify the discussion, a description of the physical system and mathematical formulation will be provided. In Fig. 1, the flow configuration is shown. A jet flapped transonic airfoil *AEBD* is depicted with a jet sheet, *BFGD* exhausting behind it as a result of momentum flux ejected through region *EBD*. Referring to the axis system, the upper and lower surfaces of the airfoil are given by

$$\alpha(x+1)+y(x)=\begin{cases}\delta f_u(x)=\delta[c(x)+t(x)],\\ -1\le x\le 1,\\ \delta f_\ell(x)=\delta[c(x)-t(x)]\end{cases}$$

where x and y are nondimensional coordinates, chosen so that the basic chord length is 2 and the thickness is 2δ. Thus, δ is the usual thickness ratio; $c(x)$ and $t(x)$ are the camber and thickness functions, respectively, and are normalized so that

$$\max_{-1\le x\le 1}|f_u(x)-f_\ell(x)| = 2\max_{-1\le x\le 1}|t(x)| = 2$$

The function f is arbitrary, and the subscripts u and ℓ denote upper and lower surfaces, respectively. Letting M_∞ be the freestream Mach number and α be the angle of attack shown in Fig. 1, the transonic similarity parameters K and A are defined as

$$K=(1-M_\infty^2)/M_\infty\delta^{2/3} \text{ and } A=\alpha/\delta$$

In a transonic small disturbance limit process, where the quantities δ and $\alpha\to 0$, with x, $\bar{y}=(M_\infty^2\delta)^{1/3}y$, A and K fixed,

Received July 17, 1975; presented as Paper 75-82 at the AIAA 13th Aerospace Sciences Meeting, Pasadena, Calif., Jan. 20-22, 1975; revision received Feb. 20, 1976. The authors wish to express their gratitude to H. Yoshihara and R. Magnus for providing the experimental results incorporated in this paper.

Index categories: Subsonic and Transonic Flow; Jets, Wakes, and Viscid-Inviscid Interactions.

*Program Manager—Fluid Dynamics, Science Center. Associate Fellow AIAA.

†Member of Technical Staff, Science Center.

in a nearly sonic freestream, the perturbation potential ϕ is given by‡

$$[(K-(\gamma+1)\phi_x]\phi_{xx}+\phi_{\bar{y}\bar{y}}=0 \tag{1a}$$

$$\phi_{\bar{y}}(x,0\pm)=f'_{u,\ell}(x)-A \quad |x|\leq 1 \tag{1b}$$

$$\phi_x,\phi_{\bar{y}}\to 0 \text{ as } x^2+\bar{y}^2\to\infty \tag{1c}$$

where γ, the ratio of the specific heats, is assumed constant and the small disturbance formulation allows a transfer of the boundary conditions to the x axis. The subsidiary conditions involving the boundary $\epsilon(x)$ of the jet for $x>1$ may be written as

$$[\phi_x]\equiv\phi_x(x,0+)-\phi_x(x,0-)=C_\mu\epsilon''(x) \tag{2a}$$

$$\phi_y(x,0\pm)=\epsilon'(x) \tag{2b}$$

The quantity C_μ is a transonically scaled blowing coefficient. If J=jet momentum flux per unit span, q=freestream dynamic pressure, and L is the airfoil chord, the blowing coefficient C_j is typically defined as

$$C_j=J/qL$$

According to transonic similarity,

$$C_\mu=M_\infty^{3/4}\delta^{1/3}C_j$$

The remaining boundary conditions on the jet boundary, which is "free" in the sense that it interacts with the solution, are

$$-\epsilon'(1)=A+\tau/\delta,\ \epsilon(1)=\epsilon'(\infty)=0 \tag{2c}$$

Here, τ is the jet deflection angle. Thus, the idealized boundary-value problem obtained using Eqs. (1) and (2) for a finite rectangular region in the scaled physical plane, is shown in Fig. 2. A far-field boundary condition $\phi=\phi_{FF}$ also is depicted, which is to be used to reduce the size of the numerical problem.

Integrodifferential Equation and Far Field

In this section, the function ϕ_{FF} will be determined in terms of an integrodifferential equation. For this purpose, it will be convenient to work in a rescaled coordinate system given by

$$x^\dagger=x$$

$$y^\dagger=\sqrt{K}\bar{y}$$

In these variables, the transonic potential equation (TPE) expressed in nonlinear Poisson form is

$$\Delta\phi=[(\gamma+1)/2K](\partial u^2/\partial x) \tag{3}$$

where, upon dropping the daggers,§ $\Delta\equiv\partial^2/\partial x^2+\partial^2/\partial y^2$ and $\nabla\phi\equiv(u,v)$.

Consider a region R, bounded by a large rectangle with cuts along the airfoil, and any possible shocks, such as S_1 and S_2 shown in Fig. 3. Denote the periphery, including the cuts, by Λ. Green's formula applied to the region R is

$$\oint_\Lambda(U\partial V/\partial n-V\partial U/\partial n)\mathrm{d}s=\iint_R(U\Delta V-V\Delta U)\mathrm{d}A \tag{4}$$

‡The definition of K given in Eq. (1.1.11) of Ref. 8 was employed to obtain Eq. (1a). However, the altered definition was also used as indicated to improve agreement with experiment.

§These will be discarded without confusion in what follows.

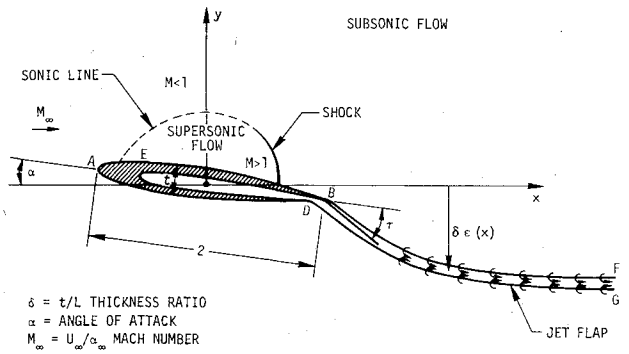

Fig. 1 Flowfield configuration.

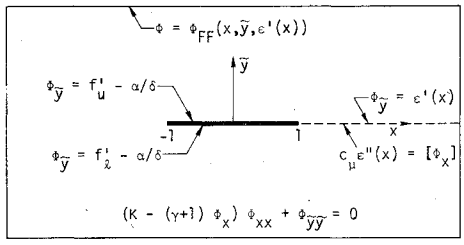

Fig. 2 Mathematical formulation.

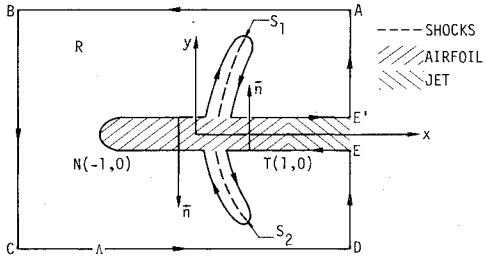

Fig. 3 Region for application of Green's theorem.

where the left-hand member is a counterclockwise integration, and $\partial/\partial n$ is the normal derivative in the direction of the outward normal, ds is the differential arc length, and dA is the area element. Denoting the field point as $P(x,y)$, the test point as $Q(\xi,\eta)$, and $\delta(P,Q)$ as the two-dimensional delta function, a Green's function $G(P,Q)$ is defined, having the properties

$$\Delta G=\delta(P,Q) \tag{5a}$$

and

$$\partial G/\partial n=0 \tag{5b}$$

on the semi-infinite slit $ETNE'$ in Fig. 3. The advantage of the imposition of Eq. (5b) is that it eliminates certain boundary terms in the application of Eq. (4) to obtain an integral representation for ϕ. The presence of the jet in this problem, does not affect the arguments given in Krupp[8] establishing that the contributions on the shock slits S_1 and S_2 in Fig. 3 vanish. Denoting the jump and mean of some function $f(x,y;\xi,\eta)$ across the ξ axis, respectively, as

$$[f]\equiv f(x,y;\xi,0+)-f(x,y;\xi,0-)$$

$$f^*\equiv(f(x,y;\xi,0+)+f(x,y;\xi,0-))/2$$

then the jump in the product of f and another function g is

$$[fg]=[f]g^*+f^*[g] \tag{6}$$

Under the assumption that ϕ decays sufficiently fast as $\xi^2+\eta^2\to\infty$, the contribution to the line integral in Eq. (4) on $E'ABCDE$ vanishes, if $\phi=U$, and $G=V$. Use of this fact, together with Eqs. (5) and (6) in Eq. (4), leads to the form

$$\phi=\frac{1}{\sqrt{K}}\int_{-1}^{\infty}[Gv]\,d\xi+\frac{\gamma+1}{2K}\int_{-\infty}^{\infty}\int_{-\infty}^{\infty}u^2\frac{\partial G}{\partial\xi}d\xi d\eta \qquad (7)$$

In order to obtain G, the slit is unfolded with the conformal mapping

$$w=(z+1)^{1/2} \qquad (8a)$$

where

$$z\equiv x+iy=re^{i\theta} \quad w=s+it$$

$$\zeta\equiv\xi+i\eta=\rho e^{i\phi} \quad w_0=s_0+it_0 \qquad (8b)$$

and the branch cut for the square root is on the interval $[-1,\infty)$, i.e., $0\le\arg(z+1)<2\pi$. The correspondences under Eq. (8) are shown in Fig. 4, where like shadings represent mappings of each other. Thus, the cut z plane is mapped into the upper half of the w plane, with the primed points as mappings of the unprimed quantities in the z plane. If a complex function Ω is defined such that $Re\Omega=G$, on NE, or arg $(z+1)=0$, the following relation holds:

$$-\partial G/\partial n_Q=\partial G/\partial\eta=(1/2s)\,d\Omega/dw_0 \qquad (9)$$

If Eq. (5b) is satisfied in the w plane, Eq. (9) guarantees that it will be valid in the z plane. By the reflection principle, it is seen easily that

$$2\pi\Omega(P,Q)=\log(w_0-w)+\log(w_0-\bar{w})$$

or, on taking the real part,

$$G(P,Q)=(1/2\pi)\log|(w_0-w)(w_0-\bar{w})| \qquad (10)$$

Using the properties of Eq. (8a), it can be shown that

$$[G(Q,P)]=(-2/\pi)Re\coth^{-1}[(\xi+1)/(z+1)]^{1/2} \qquad (11a)$$

$$G(Q,P)^*=(1/2\pi)\log|z-\xi| \qquad (11b)$$

From Eqs. (1) and (4)

$$[v]=2t'(\xi) \qquad (11c)$$

$$v^*=c'(\xi)-A \qquad (11d)$$

Substitution of Eq. (11) into Eq. (7) gives

$$\phi=\frac{1}{\pi K^{1/2}}\left\{\int_{-1}^{1}t'(\xi)\log|z-\xi|\,d\xi+\int_{-1}^{1}R(z,\xi)[c'(\xi)-A]\,d\xi+\int_{1}^{\infty}R(z,\xi)\epsilon'(\xi)\,d\xi\right\}+\frac{\gamma+1}{2\pi K}\int_{-\infty}^{\infty}\int_{-\infty}^{\infty}u^2(\xi,\eta)\frac{\partial G}{\partial\xi}d\xi d\eta \qquad (12a)$$

where the kernel $R(z,\xi)$ is given by

$$R(z,\xi)=\log\left|\frac{(\xi+1)^{1/2}-(z+1)^{1/2}}{(\xi+1)^{1/2}+(z+1)^{1/2}}\right| \qquad (12b)$$

Equations (12) are used in a similar empirical manner to that employed in Krupp.[8] The nonlinear double integral term in Eq. (12a) is neglected, and the remaining linear portion is used as ϕ_{FF}. A critique of this step, in the light of formal asymptotic developments for ϕ as $z\to\infty$, is given in the Appendix.

It should be noted that, in the linear case, the first three integrals appearing in Eq. (12a) represent the effect of a line source and vortex, respectively, as can be seen from application of the Plemelj formulas for Cauchy integrals.[12] This gives the following reciprocity relations:

$$\frac{1}{2i}\int_{-1}^{\infty}\frac{[u]\,d\xi}{z-\xi}=-\frac{1}{(z+1)^{1/2}}\int_{-1}^{\infty}\frac{(\xi+1)^{1/2}v^*}{z-\xi}d\xi \qquad (13a)$$

$$\frac{1}{i(z+1)^{1/2}}\int_{-1}^{\infty}\frac{(\xi+1)^{1/2}u^*d\xi}{z-\xi}=\frac{1}{2}\int_{-1}^{1}\frac{[v]\,d\xi}{z-\xi} \qquad (13b)$$

Equation (13a) relates the vorticity and downwash on the x axis.

Numerical Procedure

The computational method uses finite-difference techniques, employing four basic operators (parabolic, elliptic, hyperbolic, and shock-point) in the standard line relaxation iterative method originally developed by Murman.[13] A variable grid is embedded in a rectangular region enclosing the airfoil appropriate to accurate monitoring of large gradients near the nose and trailing edge singularities (see Fig. 5). Because of these singularities, no grid points lie on the vertical line passing through the nose or trailing edge of the airfoil. The boundary condition [Eq. (1b)] is incorporated into the finite-difference operators in the same manner as that explained in Murman and Cole.[10]

Since the slope of the jet $\epsilon'(x)$ is unknown at the outset, the far-field Dirichlet boundary condition ϕ_{FF} described in the previous section and Eq. (12) must be updated after each complete relaxation sweep through the grid network. The first two integrals in Eq. (12) are computed initially, and the third is decomposed as follows:

$$\int_{1}^{\infty}R(z,\xi)\epsilon'(\xi)\,d\xi=\int_{1}^{L}R(z,\xi)\epsilon'(\xi)\,d\xi+\int_{L}^{\infty}R(z,\xi)\epsilon'(\xi)\,d\xi \qquad (14)$$

where L represents the right boundary of the computational grid. Since the last term on the right-hand side of Eq. (14) contains a significant contribution of the far field, the asymptotic behavior of the jet slope given by Eq. (A6) in the Appendix is used. Upon mapping the interval $[L,\infty)$ into $[0,1/(L+1)^{1/2}]$, the tail of the infinite integral becomes

$$\int_{L}^{\infty}R(z,\xi)\epsilon'(\xi)\,d\xi\sim\frac{-K^{1/2}\Gamma}{2\pi}\int_{0}^{1/(L+1)^{1/2}}H(z,u)\,du$$

where

$$\Gamma=[\phi]_{x=1-}-C_\mu\epsilon'(1)$$

and

$$H(z,u)=\frac{2}{u(1-u^2)}\log\left|\frac{1-u(z+1)^{1/2}}{1+u(z+1)^{1/2}}\right|$$

The last finite integrals are computed initially for each far-field point z by using 32-point Gaussian quadratures, and are rescaled after each relaxation cycle using the updated value of the circulation Γ. The first integral on the right in Eq. (14) is integrated using the trapezoidal rule, starting with an initial guess for the jet slopes. These slopes then are updated after each relaxation sweep by one of two methods, depending on the magnitude of C_μ. The most advantageous of these techniques, from a programming standpoint, employs the flow tangency relation (2b) as a Neumann boundary condition on the jet, and uses the same difference operator as that employed on the airfoil. This leads to a uniform Neumann boundary condition on the inteval $[-1,L]$, eliminating the need for grid points on the x-axis. After each relaxation cycle, the jump vorticity relation (2a) is numerically integrated twice to

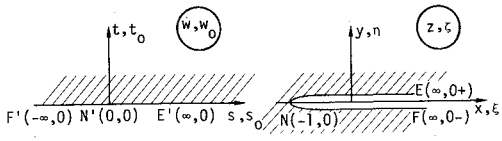

Fig. 4 Correspondences under Eq. (8a).

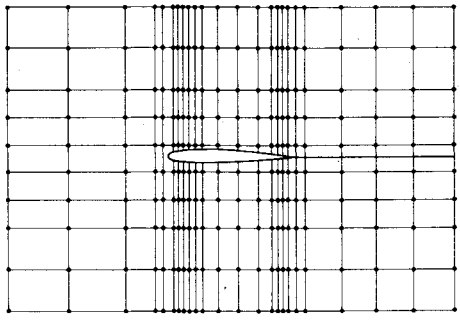

Fig. 5 Computational grid.

obtain an updated jet slope and position. Unfortunately, as $C_\mu \to 0$, the grid along the jet has to be intolerably small before acceptable accuracy is obtained. In practice, this method is limited to values of $C_\mu \geq 0.2$.

The second approach reverses the order in which the relations (2b) and (2a) are employed. For this purpose, Eq. (2a) is integrated with respect to x to obtain

$$[\phi] = [\phi]_{x+1+} + C_\mu [(\epsilon'(x) - \epsilon'(1)] \tag{15}$$

Since Eq. (1a) is valid at $y = 0+$ and $0-$, addition yields

$$[K - (\gamma+1)\phi_{x0+}]\phi_{xx0+} + [K - (\gamma+1)\phi_{x0-}]\phi_{xx0-} + \phi_{\bar{y}\bar{y}0+} + \phi_{\bar{y}\bar{y}0-} = 0 \tag{16}$$

Letting $\bar{y}_j = jh$, where h is the mesh width, and applying Taylor's theorem from above ($\bar{y}_1$) and below ($\bar{y}_{-1}$), gives

$$\phi_{\bar{y}\bar{y}0+} + \phi_{\bar{y}\bar{y}0-} = 2(\phi_{i,1} + \phi_{i,-1} - \phi_{i,0+} - \phi_{i,0-})/h^2$$
$$+ \ldots \approx 2\{\phi_{i,1} + \phi_{i,-1} - 2\phi_{i,0-} - [\phi]_{x=1+}$$
$$- C_\mu [\epsilon'(x_i) - \epsilon'(1)]\}/h^2 \tag{17}$$

where Eq. (15) has been used in the last step. The first and second expressions in Eq. (16) may be discretized in the usual way; however, Eq. (15) must be used to eliminate all unknowns evaluated at $y = 0+$. It can be verified easily that the resulting expression reduces to that of Krupp[8] when $C_\mu = 0$.

After each relaxation sweep, Eq. (2b) is applied to update the jet slope. This second method is particularly advantageous in the transonic regime when C_μ is small, i.e., $0 \leq C_\mu \leq 0.2$.

In contrast to the pure lifting airfoil program, the jet flap routine requires three different choices for the relaxation parameter ω. Underrelaxation ($0.7 \leq \omega \leq 0.9$) is applied whenever the hyperbolic, parabolic, or shock-point operator is encountered; otherwise, slight overrelaxation ($1. \leq \omega \leq 1.2$) is used in the jet region ($x > 1$), and overrelaxation ($1.0 \leq \omega \leq 1.9$) is applied elsewhere. When large values of ω were used in the jet region, the iterative method diverged. It is believed that this is due to instabilities created by the jet slopes changing each iteration.

Our program uses three grid networks—crude (about 2000), medium (about 3500), and fine (about 5000)—with each having many points in the vicinity of the trailing edge in order to alleviate the problem of the change in the circulation lagging behind the maximum residual; a difficulty encountered by Ives and Melnik.[7] Most of the work to obtain an accurate value of the lift is done by use of the more efficient crude mesh. Once this value has converged, a more accurate pressure distribution can be obtained by automatically switching to medium and, finally, to the fine grid. A typical run to reduce the maximum residual, the change in circulation, and the maximum error in the jet slope between successive iterations to a tolerance of 10^{-5} requires about 1500 iterations using the crude grid, followed by 200 each of the medium and fine grids. Further details of the numerical procedure, and convergence properties of the computational solution are given in Ref. 14.

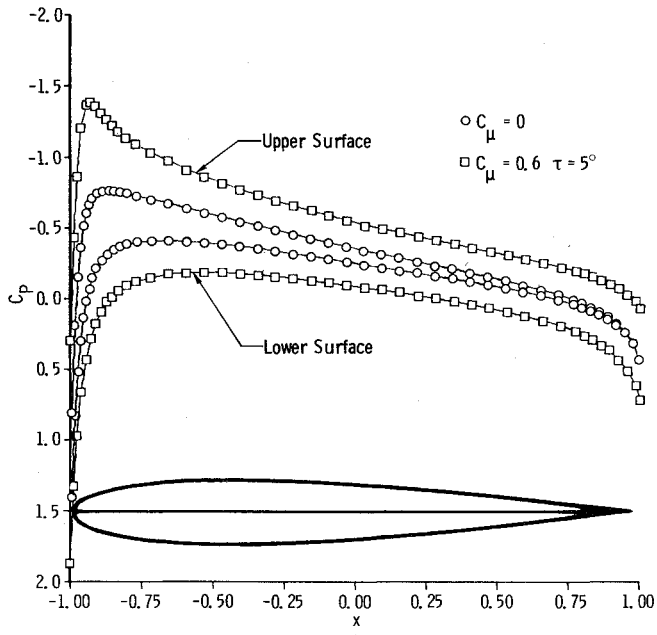

Fig. 6 Chordwise pressure distributions, NACA 0012 Airfoil with jet flap, $M_\infty = 0.6$, $\alpha = 1°$, $\tau = 5°$, $C_\mu = 0.6$.

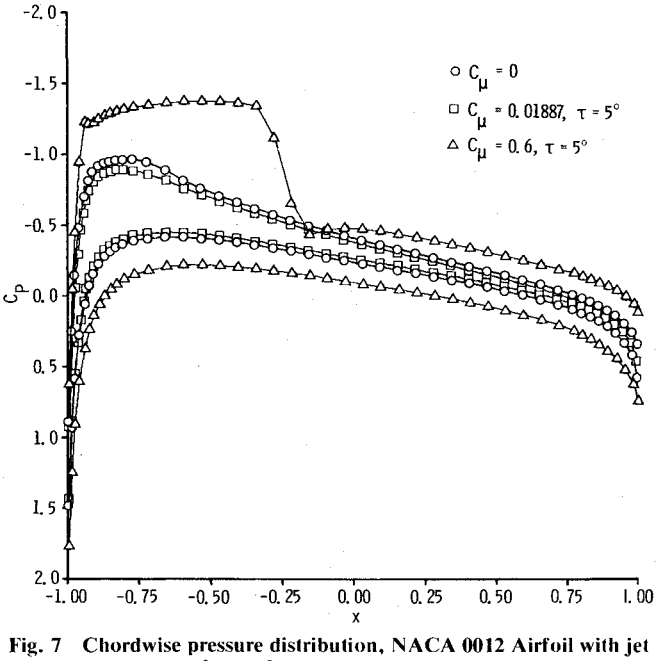

Fig. 7 Chordwise pressure distribution, NACA 0012 Airfoil with jet flap, $M_\infty = 0.7$, $\alpha = 1°$, $\tau = 5°$.

Results and Discussion

Chordwise pressure distributions with $C_p = (\delta^{2/3}/M_\infty{}^{1/4})\phi_x$ have been obtained for various airfoils, and are exemplified

for a NACA 0012 airfoil at 1° angle of attack at Mach numbers (M_∞) of 0.6 and 0.7 in Figs. 6 and 7. The jet deflection angles and blowing coefficient $C\mu$ are expressed in lumped parameters appropriate to the underlying small disturbance theory. This fact represents another important result of the present analysis—the extension of transonic similitude to jet flapped airfoils. The similarity represents another advantage of the numerical formulation within the small disturbance framework, allowing "universal curves" to be constructed for variation of lift with the Karman similarity parameter, lumped blowing, and jet deflection angle parameters.

It is evident from the result that substantial enhancement of the lifting pressures on upper and lower surfaces can be achieved with moderate amounts of blowing and relatively small jet deflection angles. For the nearly subcritical case of $M_\infty = 0.6$, the increases occur over the entire chord, but are predominant in the nose region, as shown in Fig. 6.

At $M_\infty = 0.7$, the jet flap enlarges the region of supercritical flow, and produces a shock wave at approximately the half-chord station, as shown in Fig. 7, in contrast to the pure-lifting case, which is shockless. In the forward region, the pressure for $C_\mu = 0.6$ exhibits a significant plateau in the supersonic region. Pressures also are shown for much smaller blowing, typical of transonic applications ($C_j = 0.05$). These results were obtained by the second approach, described previously, and illustrate the continuity of the numerical solution with respect to C_μ as that quantity tends to zero.

For all Mach numbers, the jet effect produces a pressure difference at the trailing edge, reflecting the absence of the Kutta condition, which is applicable to the pure lifting case.

In Fig. 8, the benefits of the jet flap are shown for a modified NACA 64A406 airfoil[15] at $M_\infty = 0.7$ and $\alpha = 1°$. In addition to the lifting pressure enhancement and the discontinuity at the trailing edge produced by the jet at $C_\mu = 0.465$ and $\tau = 5°$, there appears to be considerable increase in the suction peak at the nose due to the blowing.

A byproduct of the numerical solution is the jet contour $\epsilon(x)$. A typical plot is shown in Fig. 9 for a NACA 0012 airfoil. The general shape is monotonic, and qualitatively resembles those in the incompressible regime, particularly for $x \to \infty$, in accord with the development in the Appendix. This information is of significance in connection with wing-tail interference.

In order to validate the elliptic difference algorithm, the numerical method was compared to the analytical solution for a subcritical flat plate with and without a jet flap. For $M_\infty = 0.4$, and $\alpha = 0.05$ rad, the chordwise pressures for the pure lifting case are shown in Fig. 10. The agreement between analytical and unblown numerical solutions is excellent except at the nose, where the leading singularity is not captured by the numerical method. In spite of this problem, the lift coefficient, which was computed from the circulation Γ rather than pressure integration, agreed to three significant figures with that given by the analytical solution. As a frame of reference, the corresponding jet flap solution using the numerical procedure of this paper for $\tau = 0.1$ rad and $C_j = 2$ is shown, demonstrating the enhancement in lifting pressures.

In Fig. 11, the authors' numerical solution is compared with a subsonically scaled version of Spence's analytical results. Only the linear subcritical case is considered here. The scaling law was derived in the usual way, from the appropriate affine transformation relating the incompressible to compressible free boundary value problem. This procedure leads to the following scaling laws.

Pressure Coefficient

$$C_{P_{M=0}} \equiv F(x;\alpha,\tau,\delta,C_j) \tag{18a}$$

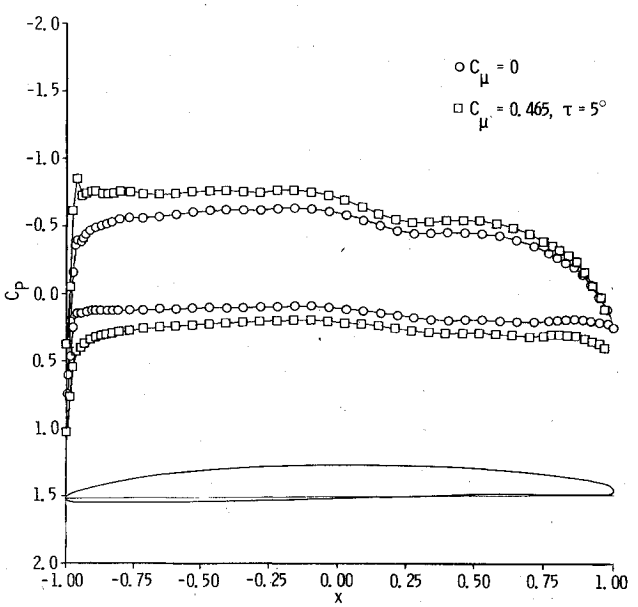

Fig. 8 Chordwise pressure distribution, NACA 64A406 (MOD) Airfoil with jet flap, $M = 0.7$, $\alpha = 1°$.

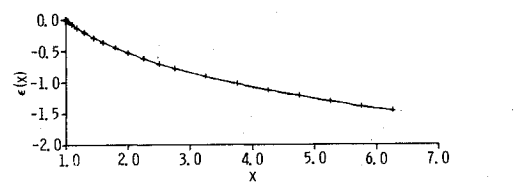

Fig. 9 Jet shape for NACA 0012 Airfoil with jet flap, $M_\infty = 0.7$, $\alpha = 1°$, $\tau = 5°$, $C_\mu = 0.6$.

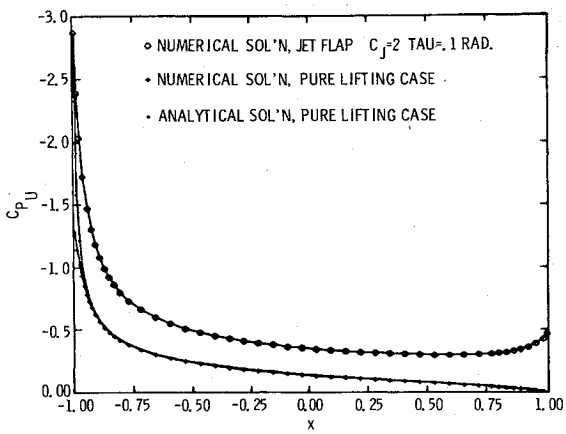

Fig. 10 Comparison of numerical and analytic solutions for subcritical flat plate with jet flap, $M_\infty = 0.4$, $\alpha = 0.05$ rad, $\tau = 0.1$ rad, $C_j = 2$.

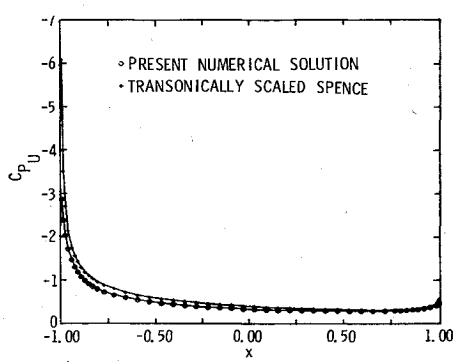

Fig. 11 Comparison of numerical solution of this paper with subcritically scaled Spence[2] solution for jet flapped flat plate, $M_\infty = 0.4$, $\alpha = 0.05$ rad, $\tau = 0.1$ rad, $C_j = 2$.

$$2C_{P_{M\neq 0}} = \tau^{2/3} M_\infty^{-3/4} F(x; 2AK_1^{-1/2}, \quad 2K_1^{-1/2}$$

$$2A'K_1^{-1/2}, M_\infty^{3/4}\tau^{1/3}C_jK_i^{1/2}) \tag{18b}$$

$$A \equiv \alpha/\tau \quad A' \equiv \delta/\tau \quad K_1 \equiv (1-M_\infty^2)/M_\infty \tau^{2/3} \tag{18c}$$

Lift Coefficient

$$C_{L_{M=0}} = 2\int_0^1 F(x;\alpha,\tau,\delta,C_j)\,dx$$

$$\equiv \lambda(\alpha,\tau,\delta,C_j) \tag{18d}$$

$$2C_{L_{M\neq 0}} = \tau^{2/3} M_\infty^{1/4} \lambda(2AK_1^{-1/2}, 2K_1^{-1/2}$$

$$2A'K_1^{-1/2}, M_\infty^{1/4}\tau^{1/3}C_jK_1^{1/2}) \tag{18e}$$

where the δ dependence in Eq. (18) is to be omitted in the specialization to the flat plate case. Noting that F and λ are linear functions of the first three parameters, Eqs. (18b) and (18e) specialize¶ to the Prandtl Glauert forms

$$C_{P_{M\neq 0}} = F\left(x, \frac{\alpha}{\beta}, \frac{\tau}{\beta}, \frac{\delta}{\beta}, \beta C_j\right)$$

$$C_{L_{M\neq 0}} = \lambda\left(\frac{\alpha}{\beta}, \frac{\tau}{\beta}, \frac{\delta}{\beta}, \beta C_j\right)$$

$$\beta \equiv (1-M_\infty^2)^{1/2}$$

which are consistent with the results obtained in Refs. 16 and 17 for the special case of $\delta = 0$.

Agreement between numerical and the scaled solution of Spence[2], using Eqs. (18b) and (18e), is reasonably good with some degradation in the vicinity of the nose. As in the pure lifting case. This is at least partially because of the singularity at the leading edge. An additional factor affecting the discrepancies is the arbitrariness in the selection of the scaling parameters (the Spreiter method was used in this connection). As for the pure lifting case, the value of the blown C_L calculated from the numerically determined circulation, rather than the pressures, agreed with the analytical result to three significant figures.

In Fig. 12, measured pressures over an unblown, 10% thick, aft cambered airfoil tested by Yoshihara and his coworkers at $M_\infty = 0.766$ and $\alpha = 1.21°$ in the NAE tunnel in Ottawa are compared with the $C_\mu = 0$ specialization of the algorithm of this paper. The quality of the agreement is quite good considering the nose bluntness, and the fact that no attempt was made to account for tunnel wall and viscous effects. A corresponding comparison is given in Fig. 13, for the same airfoil in the blown configuration, with $M_\infty = 0.761$, $\alpha = 1.18°$, $\tau = 85°$, and $C_j = 0.0217$. Considering the size of τ, and the limitations of small disturbance theory, the agreement on the lower surface is quite surprising. One explanation may lie in relief of the forward-facing step effect by jet entrainment. In addition, rapid curvature of the jet may reduce the effective jet angle sensed upstream. Empirical models employing specified pressures over the upper surface of a thickened wake have been proposed in Ref. 18. In combination with viscous and wall corrections, these should be studied toward reducing the discrepancies on the upper surface. For the unknown configuration, the calculated C_L was 0.589 as compared to the experimental value of 0.532. In the blown case, the computed result increases to 0.958 in comparison to the measured value of 0.962.

¶The M_∞ monomials in the definition of K_1 and Eq. (18) are discarded in this regime.

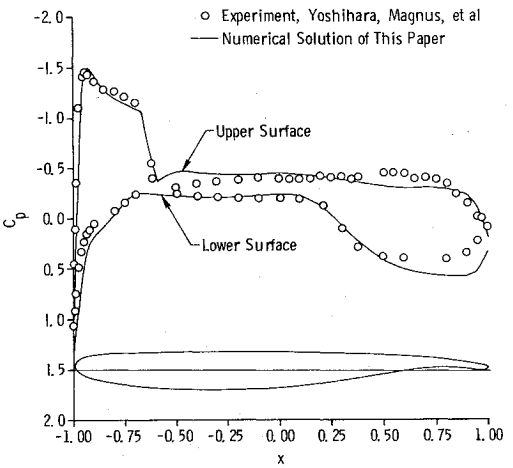

Fig. 12 Comparison of numerical solution of this paper with measurements on an aft cambered airfoil for $M_\infty = 0.766$ and $\alpha = 1.21°$.

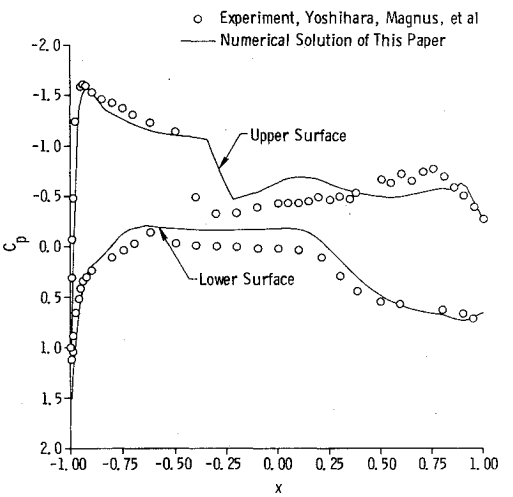

Fig. 13 Comparison of numerical solution of this paper with measurements on an aft cambered airfoil with a jet flap for $M_\infty = 0.761$, $\alpha = 1.18°$, $\tau = 85°$, and $C_j = 0.0217$.

Figure 14 compares chordwise pressures using the method in this paper against those obtained using the algorithm in Ref. 7. The agreement is reasonable everywhere except near the termination of the supersonic zone. Both shock point (fully conservative) and unconservative methods show pronounced discrepancies with the full equation method for this case in predicting the location and abruptness of the recompression to subcritical flow. Factors that may cause the disagreement may include inadequacies of the small disturbance theory in the vicinity of the nose, inaccuracies of the Spence boundary condition employed in this paper, and intrinsic difficulties of the Ives-Melnik method in treatment of the trailing-edge region. In this context, Refs. 2 and 19 indicate, however, small differences in computational solutions for a number of airfoils with and without a transfer of boundary conditions to the extended chord line for C_j's as high as 4 and $0 \leq \tau \leq 90°$. The "averaging" operator given by Eq. (17) was used to treat the discontinuous derivatives across the jet in our method. In Ref. 7, the corresponding procedure for handling these discontinuities is not discussed, and may be different from our algorithm, affecting the resolution of both sets of results. As indicated in Refs. 20 and 21, the "full" potential equation method of Jameson[22] as used in Ref. 7 and the difference methods employed in this paper** capture

**This statement holds for the nonconservative operators.

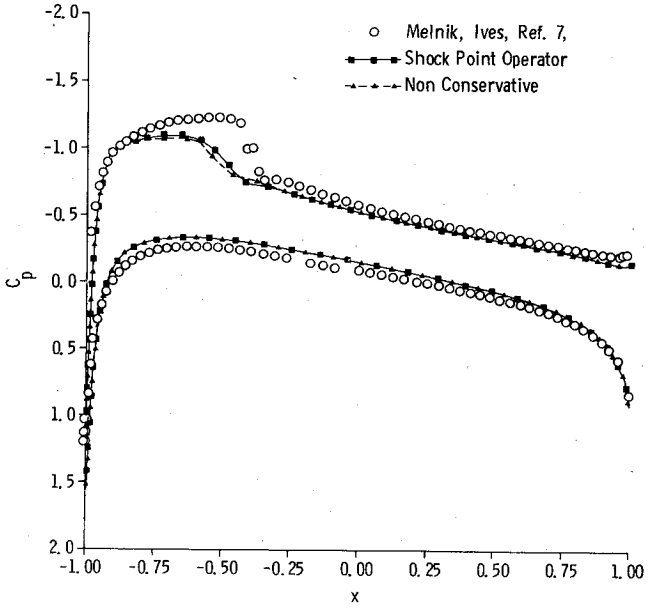

Fig. 14 Comparison of numerical solution of this paper with that of Ref. 7 for jet flapped NACA 0012 Airfoil at $M_\infty = 0.7$, $\tau = 30°$, $\alpha = 0°$, and $C_j = 0.1$.

shocks incorrectly. This aspect, as well as lack of optimality of the choice of scaling as discussed in Ref. 21, may introduce further disagreement between both sets of results. A systematic study of these aspects should be performed in the future.

Conclusions

A transonic small disturbance solution has been developed to treat the flow over supercritical jet flapped two-dimensional airfoils. Because of the successful application of a far-field boundary condition in the physical plane, flexibility in grid refinement is afforded in the treatment of leading and trailing edge singularities. In addition, the method can be generalized to handle three-dimensional flows. Typical results for NACA 0012 and 64A406 airfoils demonstrate the anticipated enhancements in lifting pressures, as well as the increase of the suction peak near the leading edge. As in incompressible flow, the structure of the field is that due to a vorticity packet, i.e., a concentrated vortex whose circulation is proportional to the total vorticity on the wing and jet. As in the pure lifting case, and in contrast to the low-speed regime, the circulation interacts nonlinearly with the field.

Appendix

A more transparent integrodifferential equation than Eq. (12) is obtained by using the fundamental solution

$$F(P,Q) = (1/2\pi)\log|z-\zeta|$$

instead of G in Eq. (4). The boundary terms, eliminated by the use of G, thus are retained. Their significance is brought out by integrations by parts, leading to

$$\phi = \frac{1}{2\pi} Re\left\{2\int_{-1}^{1} t'(\xi)\log(z-\xi)\,d\xi + i\int_{-1}^{\infty}[u]\log(z-\xi)\,d\xi + \frac{\gamma+1}{K}\int_{-\infty}^{\infty}\int_{-\infty}^{\infty}\frac{u^2(\xi,\eta)}{z-\zeta}\,d\xi d\eta\right\} \tag{A1}$$

Equation (A1) holds for the special pure lifting case ($C_\mu = 0$). Here, the only change is that the upper limit on the second integral becomes unity, reflecting the absence of vorticity $[u]$ on the wake $[1,\infty)$. This special form has been derived by Klunker.[23] It should be noted in this connection that

$$\epsilon''(x) = [u]/C_\mu = O(1) \text{ as } C_\mu \to 0$$

In Eq. (A1), the first and second terms correspond to source and vortex distributions, respectively. Upon integration by parts

$$I_1 \equiv \int_{-1}^{1} t'(\xi)\log(z-\xi)\,d\xi + \int_{-1}^{1} t(\xi)(z-\xi)^{-1}d\xi$$

since for closed airfoils, $t(-1) = t(1) = 0$ (to the small disturbance approximation, the jet is a massless momentum source). Expansion of the kernel for $\xi/z \to 0$, and termwise integration, gives

$$I_1 = z^{-1}\int_{-1}^{1} t(\xi)\,d\xi + z^{-2}\int_{-1}^{1}\xi t(\xi)\,d\xi + O(z^{-3}) \text{ for } z\to\infty \tag{A2}$$

Denoting I_2 as the second term in Eq. (A1), integrating by parts, subdividing the range of integration, noting that $[\phi]_{x=-1} = 0$, and assuming

$$\lim_{\xi\to\infty} C_\mu \epsilon'(\xi)\log(z-\xi) = 0$$

it follows that

$$-2\pi I_2 = \Gamma\arg z + Im\left[\int_{-1}^{1}\frac{[\phi]\,d\xi}{z-\xi} + C_\mu\int_{1}^{\infty}\frac{\epsilon'(\xi)}{z-\xi}\,d\xi\right] \tag{A3}$$

where

$$\Gamma = [\phi]_{x=1-} - C_\mu\epsilon'(1) = \int_{-1}^{\infty}[u]\,d\xi \tag{A4}$$

The finite integral in Eq. (A3) is $0(z^{-1})$ as $z\to\infty$, and the last term can be estimated by a further subdivision as follows:

$$\int_{1}^{\infty}\frac{\epsilon'(\xi)}{z-\xi}\,d\xi = \int_{1}^{a} + \int_{a}^{\infty}\frac{\epsilon'(\xi)}{z-\xi}\,d\xi \tag{A5}$$

where a is a large parameter, with $a/z = o(1)$.

The first integral on the right-hand side is given approximately by $z^{-1}\epsilon(a)$, as $z\to\infty$. Under the trial assumption that the first term in Eq. (A3) is the dominant contribution to ϕ in the far field, the jet slope would be, asymptotically,

$$\epsilon'(x) = \phi_{\bar{y}}(x,0) \doteq -\Gamma K^{1/2}/2\pi x \equiv C/x \quad \text{as } x\to\infty \tag{A6}$$

This implies that the first integral in Eq. (A5) is $cz^{-1}\log a$. If a is sufficiently large, $\epsilon'(\xi)$ can be approximated by Eq. (A6), giving

$$\int_{a}^{\infty}\frac{\epsilon'(\xi)}{z-\xi}\,d\xi \doteq \frac{C}{z}\left[\pi i - \log\frac{a}{(z-a)}\right] \doteq \frac{C}{z}\left(\log z - \log a - \frac{a}{z} + i\pi\right) + O\left(\frac{a^2}{z^2}\right) \text{ as } z\to\infty$$

Substitution of this and the previous result in Eq. (A5) gives

$$\int_{1}^{\infty}\frac{\epsilon'(\xi)}{z-\xi}\,d\xi \doteq Cz^{-1}\log z \qquad \text{as } z\to\infty \tag{A7}$$

By a similar procedure, with Schwarz's inequality and use of polar coordinates, the double integral can be found asymptotically to be given by

$$\int_{-\infty}^{\infty}\int\frac{u^2}{z-\zeta}\,d\xi d\eta \doteq \frac{\Gamma^2}{4\pi}z^{-1}\log z \tag{A8}$$

Equations (A2), (A7), and (A8), when combined, are consistent with the "vorticity packet" model for the far-field expansion

$$\phi \doteq \frac{-\Gamma\theta}{2\pi} + \frac{\log r}{r}\left[-C_\mu C\sin\theta + \frac{(\gamma+1)\Gamma^2}{8\pi^2 K}\cos\theta\right] + \ldots$$

for $z \to \infty$, as asserted previously.

References

[1] Hagedorn, M. and Ruden, P., "Windkanal Untersuchungen an Einem Junkers-Doppelflugel Mit Ausblasesschlits am Heck Des Hauptflugels," Royal Aeronautical Establishment, transl. 442, Dec. 1953.

[2] Spence, D.A., "The Lift Coefficient of a Thin Jet Flapped Wing," *Proceedings of the Royal Society*, Ser. A, Vol. 238, Dec. 1956, pp. 46-68.

[3] Lissaman, P.B.S., "A Linear Theory for the Jet Flap in Ground Effect," *AIAA Journal*, Vol. 6, July 1968, pp. 1356-1362.

[4] Sato, J., "Discrete Vortex Method of Two Dimensional Jet Flaps," *AIAA Journal*, Vol. 11, July 1973, pp. 968-973.

[5] Das, A., "Lifting Surface Theory for an Airplane Wing with a Jet Flap," German Research Institute for Aerodynamics (DFL) Rept. 093, Braunschweig 1960-NASA Technical Translation TTF-13 714.

[6] Yoshihara, H., Carter, W.V., Fatta, J.G., and Magnus, R.G., "Aeronautical Exploratory Research on Jet Flapped Airfoils," Convair Rept. L-112173, Feb. 1972.

[7] Ives, D.C. and Melnik, R.E., "Numerical Calculation of the Compressible Flow Over an Airfoil with a Jet Flap," AIAA Paper 74-542, AIAA 7th Fluid and Plasma Dynamics Conference, Palo Alto, Calif., June 17-19, 1974.

[8] Krupp, J.A., "The Numerical Calculation of Plane Steady Transonic Flows Past Thin Lifting Airfoils," Ph.D. thesis, University of Washington, Seattle, Wash., June 1971.

[9] Krupp, J.A. and Murman, E.M., "Computation of Transonic Flows Past Lifting Airfoils and Slender Bodies," *AIAA Journal*, Vol. 10, July 1972, pp. 880-886.

[10] Murman, E.M. and Cole, J.D., "Calculation of Plane Steady Transonic Flows," *AIAA Journal*, Vol. 9, No. 1, January 1971, pp. 114-121.

[11] Murman, E.M. and Cole, J.D., "Inviscid Drag at Transonic Speeds," AIAA Paper 74-540, AIAA 7th Fluid and Plasma Dynamic Conference, Palo Alto, Calif., June 17, 1974.

[12] Muskhelishvili, N.I., *Singular Integral Equations*, transl. from Russian, Groningen, P. Noordhoff, Holland, 1953.

[13] Murman, E.M., "Analysis of Embedded Shock Waves Calculated by Rleaxation Methods," *Proceedings Computational Fluid Dynamics Conference*, Palm Springs, Calif., July 19-20, 1973, pp. 27-40.

[14] Murphy, W.D. and Malmuth, N.D., "A Numerical Solution for Transonic Flow Over Supercritical Jet Flapped Airfoils," Science Center, Rockwell International Corp., Thousand Oaks, Calif., Tech. Rept., SCTR-75-8, May 1975.

[15] Grahame, W.E. and Headly, J.W., "Jet Flap Investigation at Transonic Speeds," Air Force Flight Dynamics Lab., TR-69-117, Feb. 1970.

[16] Malavard, L., "Application of the Rheoelectric Analogy for the Jet Flap Wing of Finite Span," *Boundary Layer and Flow Control*, Vol. 1, edited by G.V. Lachmann, Pergamon, New York, 1961, p. 375.

[17] Elsweig, S., "Subsonic Similarity Rule for Jet Flapped Airfoil," *Journal of Aircraft*, Vol, 8, Sept. 1971, pp. 744-745.

[18] Yoshihara, M., Magnus, R., and Zonars, D., "Transonic Drag Due to Lift of Planar Jet Flapped Airfoils," in AGARD Preprint 124, Oct. 1973.

[19] Halsey, N.D., "Methods for the Design and Analysis of Jet Flapped Airfoils," AIAA Paper 74-188, AIAA 12th Aerospace Sciences Meeting, 1974.

[20] Yoshihara, H., "A Survey of Computational Methods for 2D and 3D Transonic Flows with Shocks," General Dynamics, Convair Aerospace Div., San Diego, Calif., Rept. 6DCA-ERR-1726, Dec. 1972.

[21] Murman, E.M., Yoshihara, H., and Korn, D., "Transonic Aerodynamics Notebook," from *AIAA Professional Study Series on Transonic Aerodynamics*, 1975, pp. 10-17.

[22] Jameson, A., "Transonic Flow Calculations for Airfoils and Bodies of Revolution," Grumman Aerospace Corp., Bethpage, N.Y., Rept. 390-71-1, 1971.

[23] Klunker, E.B., "Contribution to Methods for Calculating the Flow About Thin Lifting Wings at Transonic Speeds—Analytical Expressions for the Far Field," NASA TN D-6530, Nov. 1971.